SYNTHETIC TESTS ON RESOLVABILITY OF SPACE-TIME RUPTURE HISTORY WITH ISOLA

Technical report – This is a non-peer reviewed report submitted to EarthArXiv.

Natália Verkinová [a], Jiří Zahradník [b]

[a] Charles University, Prague, Czech Republic, natalia.verkinova@gmail.com

[b] Charles University, Prague, Czech Republic, jiri.zahradnik@matfyz.cuni.cz

Abstract

This study evaluates the limitations of the ISOLA software in estimating rupture velocity by using synthetic tests that mimic the 2023 Turkish Mw 7.8 earthquake. Two types of slip-distribution models, point-like and continuous, were used as input for synthetic seismogram generation, which were then inverted using ISOLA multiple-point-source (MPS) approach. Key parameters affecting the software performance, such as earthquake source mechanism and subevent time function, were analyzed under various configurations, including different ISOLA executable versions and focal mechanism constraints. The findings underscore the limitations of ISOLA in resolving complex fault dynamics, with significant issues in both subevent timing and mechanism fidelity impacting the accurate estimation of rupture velocity.

Introduction

This study investigates the limitations of the ISOLA software (Zahradník and Sokos, 2018) in estimating rupture velocity. The study uses synthetic tests mimicking the 2023 Turkish Mw 7.8 earthquake. Input models are based on Čejka et al. (2023) and Zahradník et al. (2023). The input slip-distribution models are of two types: (i) point-like models (represented by three small slip patches), and (ii) continuous slip models. Synthetic full-wave seismograms are generated for the input models, outside ISOLA, and are inverted with ISOLA for multiple-point-source (MPS) models. The goal is to assess the resolvability potential of ISOLA in an example of a complex fault.

The primary investigated parameters affecting resolvability include the earthquake source mechanism, the versions of the ISOLA executable code (isola.exe), and the subevent time function (moment rate). Three focal-mechanism types are considered: fixed DC mechanism (prescribed by the strike/dip/rake angles), free DC-constrained moment tensor (MT), and free full MT. Two types of inversion with ISOLA are the standard ('fast') version and a modified ('slow') code version; the latter was first introduced in sec. 4.1 of Zahradník and Gallovič (2010). Two types of subevent time functions are the delta and triangle.

The considered model of a part of the East Anatolian Fault system consists of two segments: southwest (SW) and northeast (NE). The fault is discretized in 75 trial source positions (points) with a spacing of 4 km at a depth of 10 km. The transition between the two segments (i.e., the 'corner') occurs at trial position 38, situated 148 km from the SW fault end (Fig. 1). The hypocenter is located 20 km from the corner, at trial position 43, corresponding to an along-fault distance of 168 km from the SW fault end. Rupture initiates at the hypocenter and propagates bilaterally to SW and NE at a velocity of 3 km/s. The rupture pauses for 15 seconds in the hypocenter before resuming its propagation to the west, i.e., toward the corner and then to the SW segment. For the fixed mechanism, the prescribed strike/dip/rake angles (s/d/r °) are 30/90/0 and

60/90/0 on the SW and NE segments, respectively. All input models assume a 100% double-couple (DC) source.

Synthetic seismograms for input models (forward simulation) are calculated by F. Čejka with the Hybrid Integral-Composite (HIC) code of Gallovič and Brokešová (2007) in a frequency range 0.0-1.0 Hz for 21 stations (Fig. 2). Here, we use synthetics in which only the integral, deterministic part of the modeling techniques is employed. The Green's functions are calculated with AXITRA code (Coutant, 1989). The velocity model (Acarel, 2019) consists of 17 layers (Tab. 1). The inversion of synthetics in ISOLA is performed in a frequency range of 0.01-0.05 Hz. The time window for calculations during the inversions is 307.2 s (1024 points with the time step dt= 0.3 s). Green's functions are calculated with AXITRA up to Nyquist frequency (1.66 Hz), using the same velocity model as in the forward simulation. A temporal grid search is performed with the time step of 0.9 s in the range specified below.

In the results, wherever the focal mechanism of a subevent differs from the input model, the deviations are quantified by the Kagan angle (Kagan, 1991). The inversion is vulnerable to the 180° ambiguity of the rake angle, equivalent to the swapping of the P- and T-axes. Therefore, the Kagan angle of each subevent is calculated twice, with the original rake angle obtained from the inversion, and with the rake angle changed by 180°. The smaller of the two is chosen. If the smaller one is the original one, we denote it (in figures) as "True Kagan"; if not, we denote it as "Modified Kagan". Wherever in the inversions the DC percentage of the subevents differs from the input model (DC=100%), i.e., the DC% is an artifact, this false DC% is presented. Moments of subevents are expressed relative to the largest subevent of each test (relative moment = moment / maximal moment).

Input models

Point-like models

The point-like models have the input slip distribution depicted in Fig. 3. Their study involves the following six tests:

- TEST 1: FAST isola, FIXED mechanisms (two), DELTA function
- TEST 2: FAST isola, DC constrained (to have DC > 90%), DELTA function
- TEST 3: FAST isola, FULL MT, DELTA function
- TEST 4: FAST isola, FULL MT mechanism, TRIANGLE 20 s function
- TEST 5: SLOW isola, FULL MT mechanism, DELTA function
- TEST 6: SLOW isola, FULL MT mechanism, TRIANGLE 20 s function

For each test, we show in the main text the MPS model obtained by ISOLA compared to the input model. In Supplementary Material, we show details of the inversion, e.g., the retrieved focal mechanisms, identified subevents, comparison of real and synthetic data, and temporal evolution of the moment rate.

Rupture time $t(s)$ in the input model is $t = s / v + d$, where s is the along-fault distance of the slip-patch from the hypocenter (km), v is the rupture velocity (km/s) and d is the delay time (= 0 or 15 s for points situated to the east and west of the hypocenter, respectively).

Continuous slip models

The continuous slip models have the input slip distribution depicted in Fig. 4. Their study involves the following 4 tests:

- TEST 7: SLOW isola, FIXED mechanisms (two), DELTA function
- TEST 8: SLOW isola, DC constrained, DELTA function
- TEST 9: SLOW isola, FULL MT, DELTA function
- TEST 10: FAST isola, FIXED mechanisms (two), DELTA function

For tests with more complex behavior, we present additional plots illustrating DC% and Kagan's angles versus relative moment.

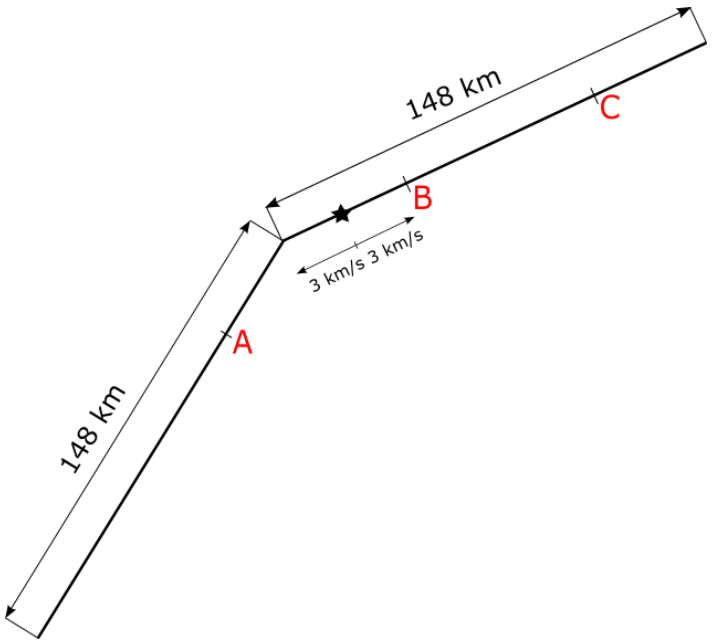

Fig. 1: **Schematic diagram of the studied fault segments.** The star represents the hypocenter, located at the NE segment. Each segment is 148 km long. Rupture propagates bilaterally from the hypocenter at a speed of 3 km/s. Before propagating west from the hypocenter, the rupture pauses for 15 seconds. Slip patches A, B, and C (subevents of the input model) are shown in Fig. 3.

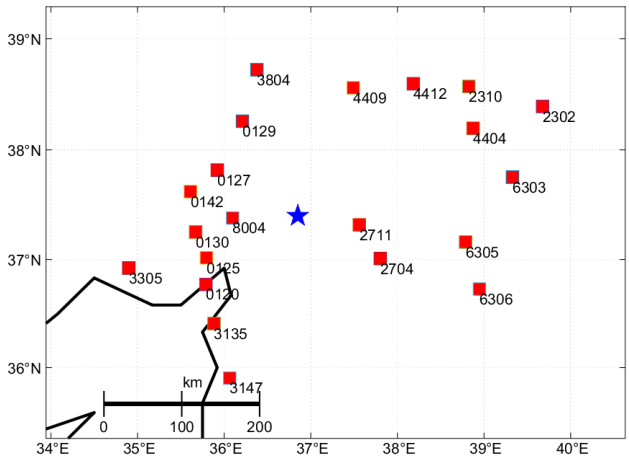

Fig. 2: **Stations used in this study.** The location and codes are those of real stations belonging to the Turkish strong-motion network AFAD. The blue star is the fault corner (not to be confused with the star depicting the hypocenter in Fig. 1).

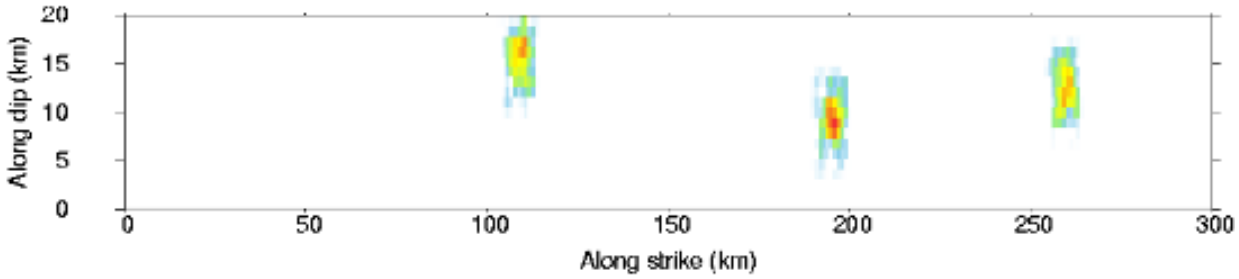

Fig. 3: **Input slip model.** The three patches, from the left to the right, are subevents A, B, and C of Fig. 1. They are located approximately at an along-fault distance of 110 km, 193 km, and 259 km from the southernmost point on the SW segment.

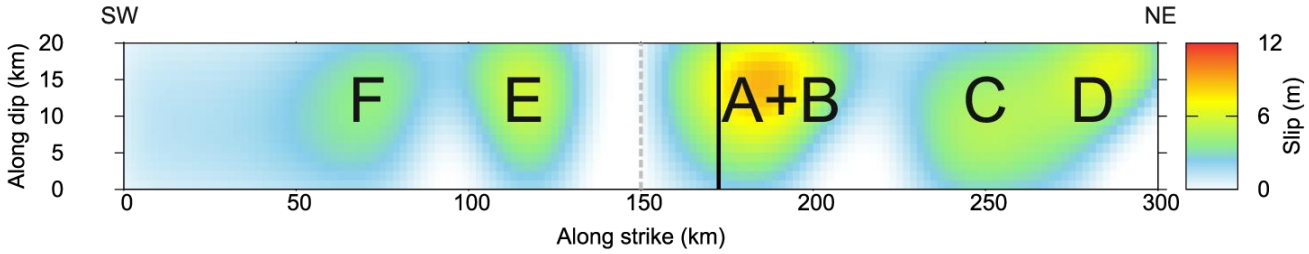

Fig. 4: **Input continuous slip model** (Čejka et al., 2023)**.** Six slip asperities are labeled A-F. The gray vertical dashed line denotes the fault corner (i.e. the transition between the SW to NE segment), while the black line depicts the hypocenter position on the NE segment.

Tab 1: **Velocity model** (Acarel et al. 2019).

Depth of layer	Vp	Vs	Rho	Qp	Qs
[km]	[km/s]	[km/s]	[g/cm^3]		
0.000	1.490	0.800	1.900	100	50
0.060	2.230	1.200	2.000	200	100
0.160	3.160	1.700	2.100	400	200
0.250	3.900	2.100	2.250	500	250
0.500	4.460	2.400	2.400	500	250
1.000	4.850	2.780	2.670	500	250
2.000	5.720	3.280	2.844	500	250
8.000	5.770	3.310	2.854	500	250
12.000	5.840	3.360	2.868	1000	500
16.000	6.080	3.520	2.916	1000	500
20.000	6.190	3.570	2.938	1000	500
24.000	6.280	3.610	2.956	1000	500
28.000	6.400	3.680	2.980	1000	500
32.000	7.400	4.180	3.180	1000	500
34.000	7.550	4.340	3.210	1000	500
38.000	7.840	4.380	3.268	1000	500

Results

Point-like slip models

TEST 1: FAST Isola model, FIXED mechanisms (two), DELTA function

Type of inversion: Fixed mechanism (s/d/r = 30/90/0, and 60/90/0 on the SW and NE segment, respectively); the transition between the segments is at trial position No. 38

Subevent time function: Delta function

Isola type: Fast

Number of subevents: 3

Number of trial source positions: 75

Temporal grid search: (-9.9, 69.9) s with step of 0.9 s

Frequency range: (0.01, 0.05) Hz

Details in the supplement: Tab. S1, Fig. S1 - S3

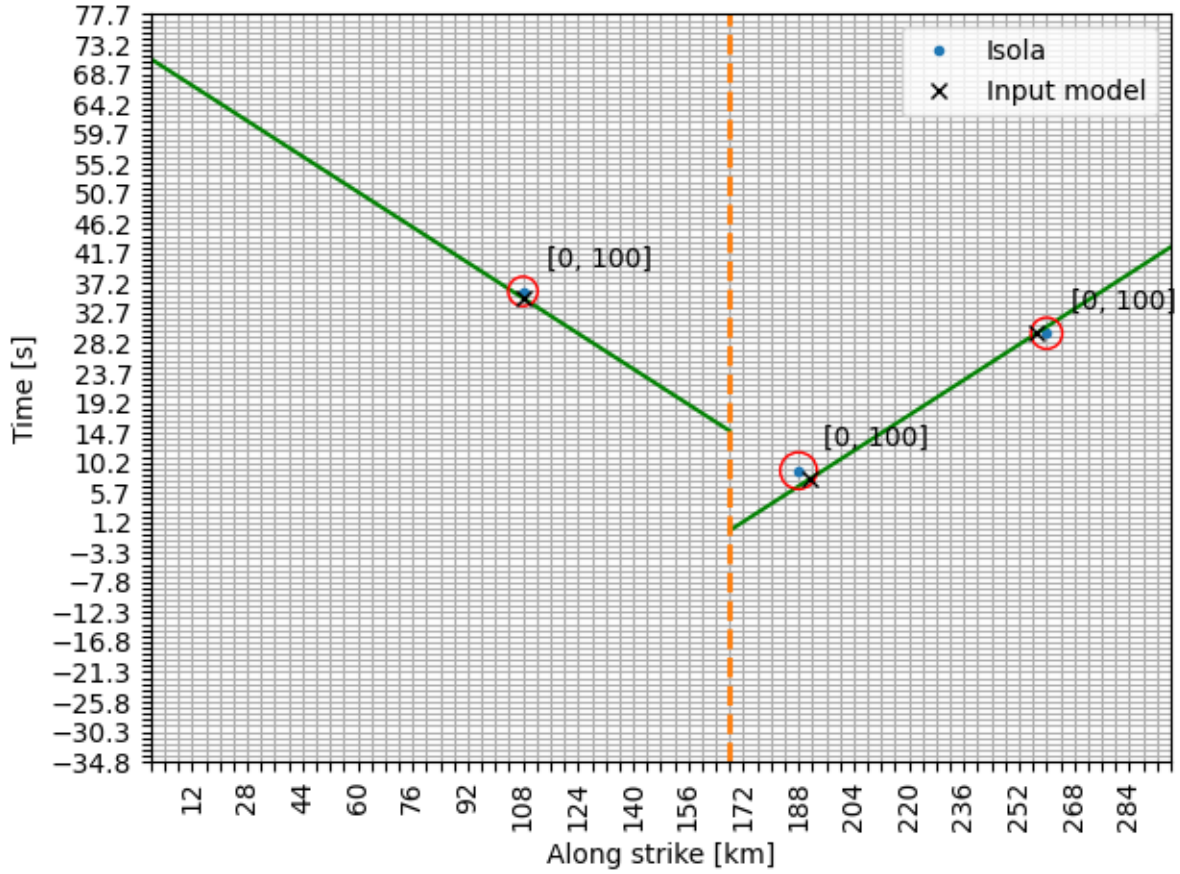

Fig. 5: **Test 1 (Point-like model. Inversion with Isola "fast", prescribed focal mechanisms, delta function).** The input model consists of three small finite sources (black crosses). Rupture propagates bilaterally at a speed of 3 km/s (green lines), with a 15-s delay in the hypocenter before propagating to the west (orange vertical dashed line). The Isola MPS model consists of three subevents (blue dots and red circles whose radius is proportional to the moment). The grid corresponds to the Isola resolution (4-km increments along the fault and 0.9-s time steps). Shown in brackets are the Kagan angle (°) and DC percentage, [K, DC%]. Input model had [0, 100].

TEST 2: FAST Isola model, DC constrained, DELTA function

Type of inversion: DC constrained; the transition between the segments is at trial position No. 38

Subevent time function: Delta function

Isola type: Fast

Number of subevents: 3

Number of trial source positions: 75

Temporal grid search: (-9.9, 69.9) s with step of 0.9 s

Frequency range: (0.01, 0.05) Hz

Details in supplement: Tab. S2, Fig. S4 - S6

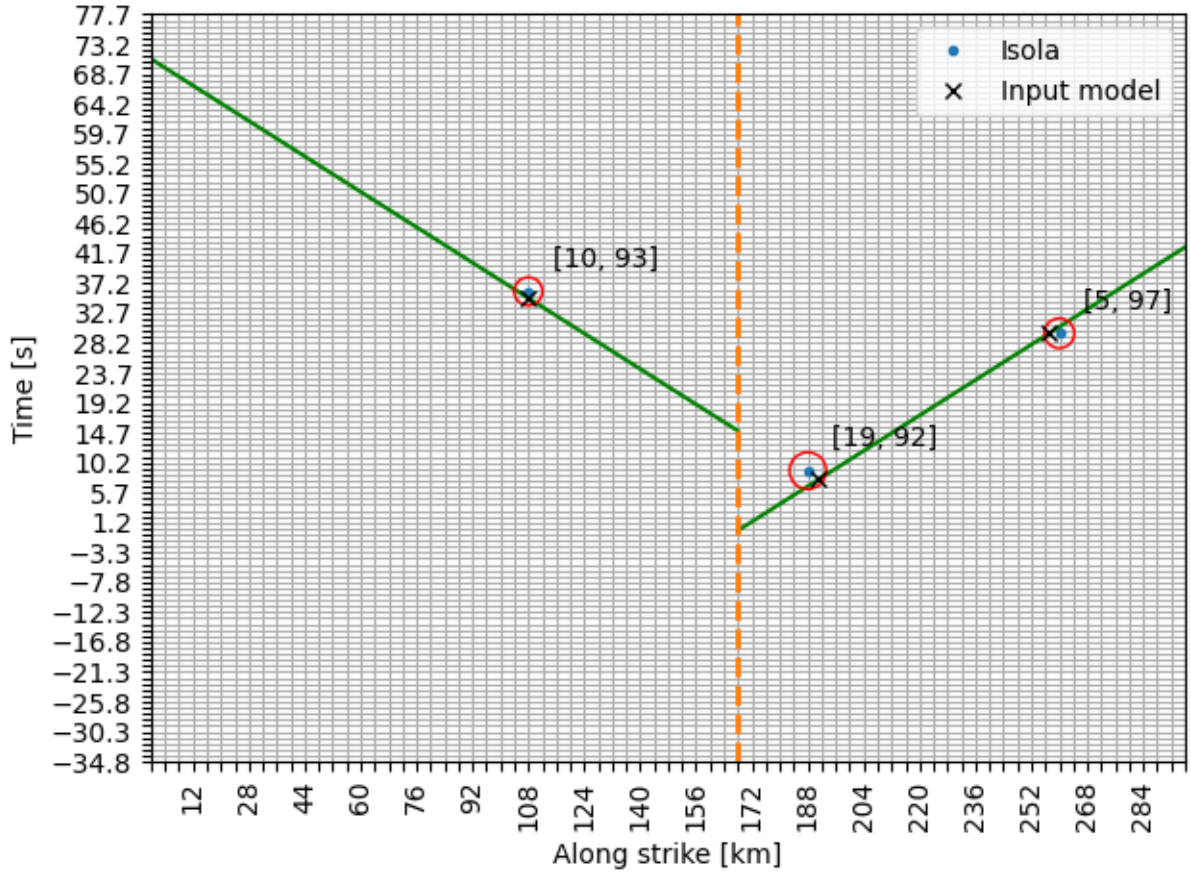

Fig. 6: **Test 2 (Point-like model. Inversion with Isola "fast", free DC-constrained mechanisms, delta function).** The symbols are the same as in Fig. 5.

TEST 3: FAST Isola model, FULL MT, DELTA function

Type of inversion: Full MT; the transition between the segments is at trial position No. 38

Subevent time function: Delta function

Isola type: Fast

Number of subevents: 3

Number of trial source positions: 75

Temporal grid search: (-9.9, 69.9) s with step of 0.9 s

Frequency range: (0.01, 0.05) Hz

Details in supplement: Tab. S3, Fig. S7 – S9

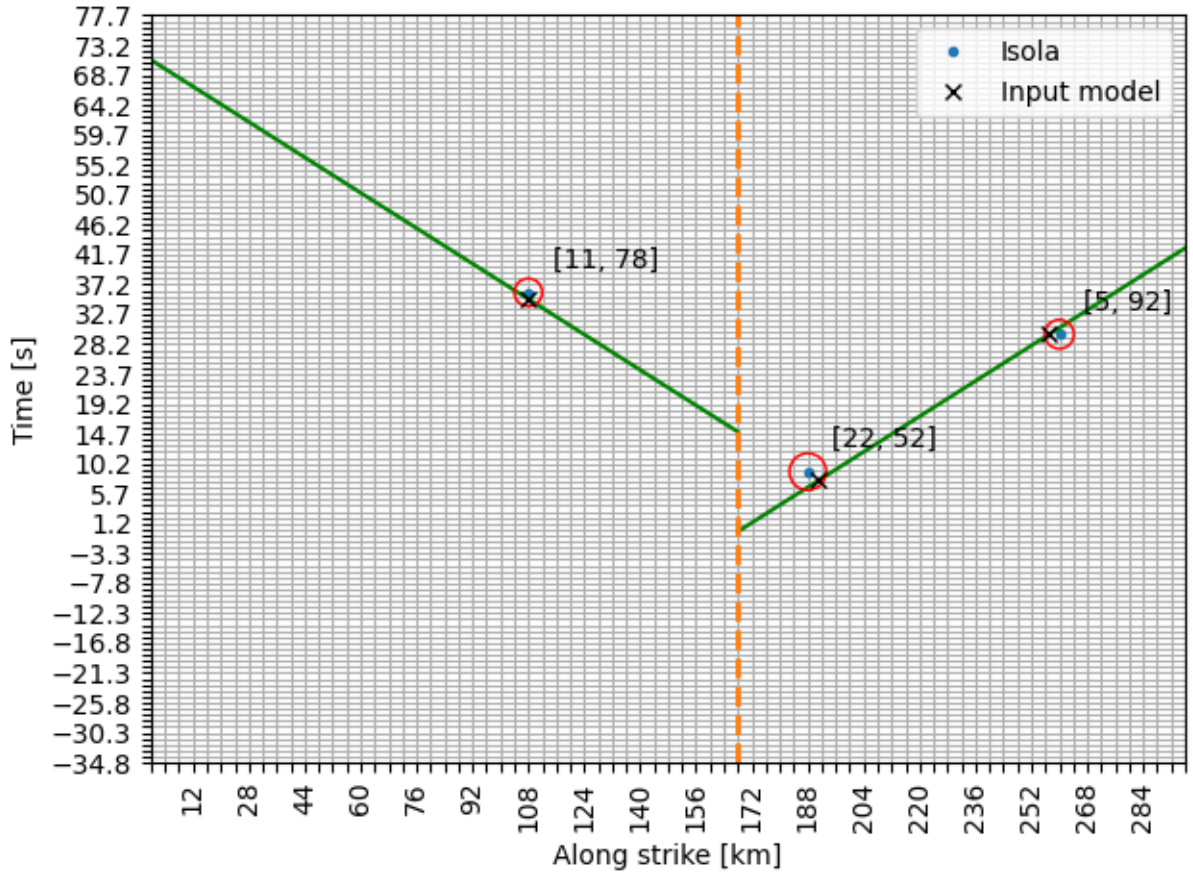

Fig. 7: **Test 3 (Point-like model. Inversion with Isola "fast", free full MT mechanisms, delta function).** The symbols are the same as in Fig. 5.

TEST 4: FAST Isola model, FULL MT mechanism, TRIANGLE 20s function

Type of inversion: Full MT; the transition between the segments is at trial position No. 38

Subevent time function: Triangle 20s function

Isola type: Fast

Number of subevents: 5

Number of trial source positions: 75

Temporal grid search: (-9.9, 69.9) s with step of 0.9 s

Frequency range: (0.01, 0.05)Hz

Details in supplement: Tab. S4, Fig. S10 - S12

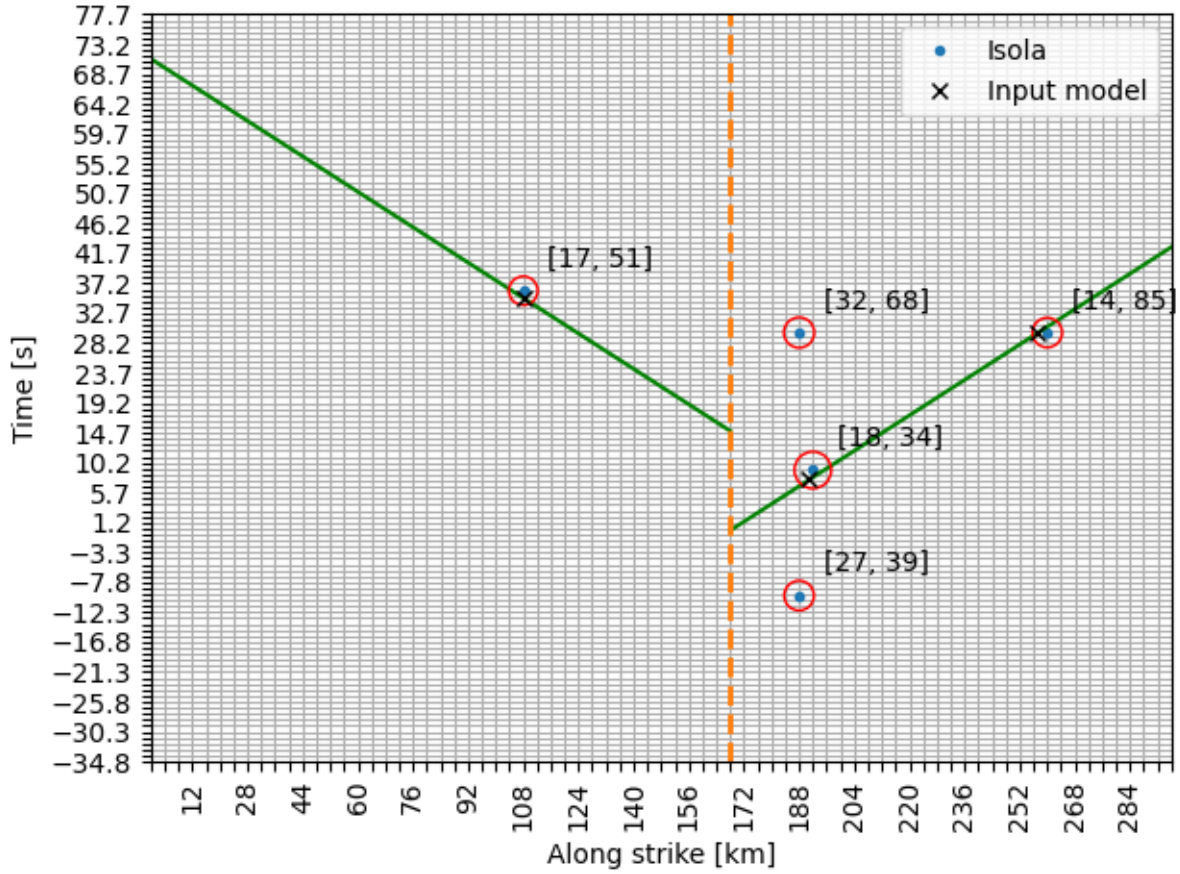

Fig. 8: **Test 4 (Point-like model. Inversion with Isola "fast", free full MT mechanisms, triangle 20-s function).** Subevent time here refers to the center of the triangle. [Note that ISOLA output reports the time of the beginning of the triangle.] The symbols are the same as in Figs. 5.

TEST 5: SLOW Isola model, FULL MT mechanism, DELTA function

Type of inversion: Full MT; the transition between the segments is at trial position No. 38

Subevent time function: Delta function

Isola type: Slow

Number of subevents: 20

Number of trial source positions: 75

Temporal grid search: (-9.9, 69.9) s with step of 0.9 s

Frequency range: (0.01, 0.05)Hz

Details in supplement: Tab. S5, Fig. S13 - S15

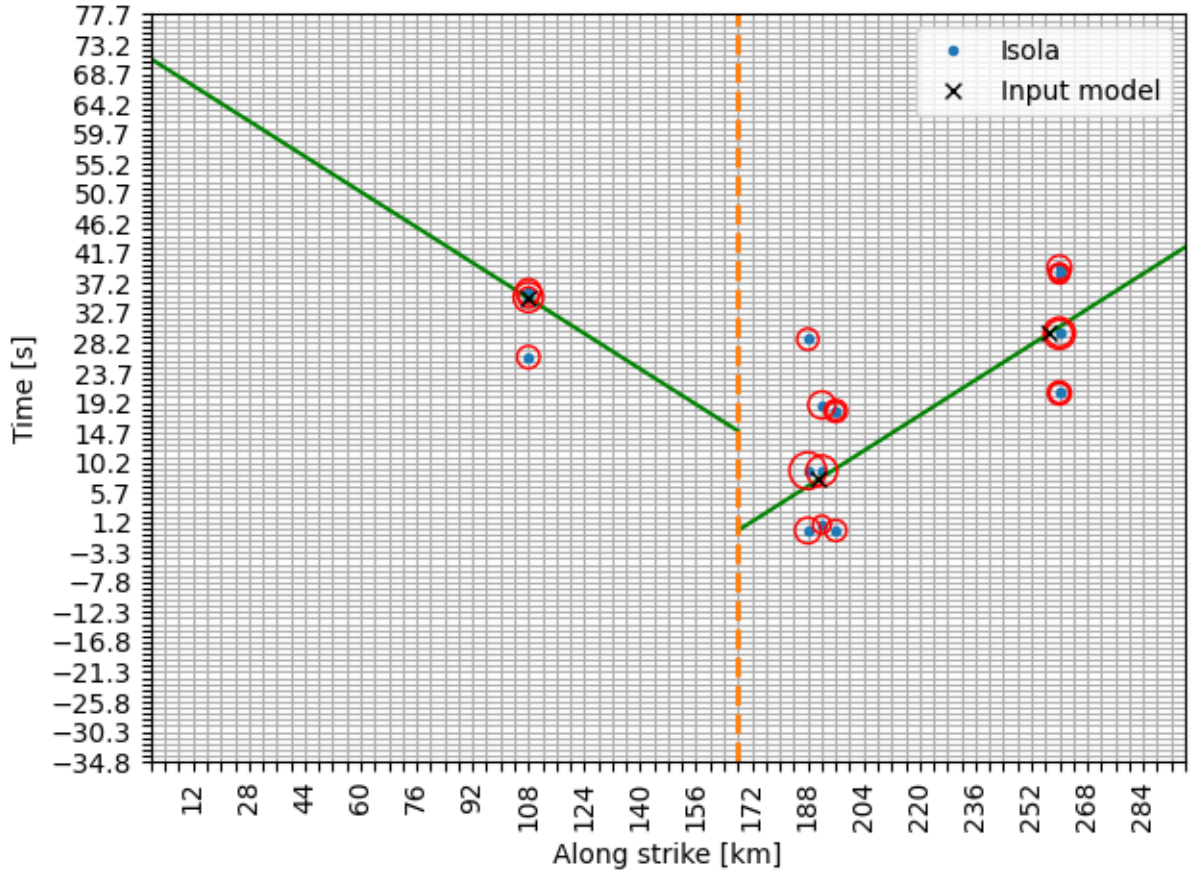

Fig. 9: **Test 5 (Point-like model. Inversion with Isola "slow", free full MT mechanisms, delta function).**

TEST 6: SLOW Isola model, FULL MT mechanism, TRIANGLE 20s function

Type of inversion: Full MT; the transition between the segments is at trial position No. 38

Subevent time function: Triangle 20s function

Isola type: Slow

Number of subevents: 20

Number of trial source positions: 75

Temporal grid search: (-9.9, 69.9) s with step of 0.9 s

Frequency range: (0.01, 0.05)Hz

Details in supplement: Tab. S6, Fig. S16 - S18

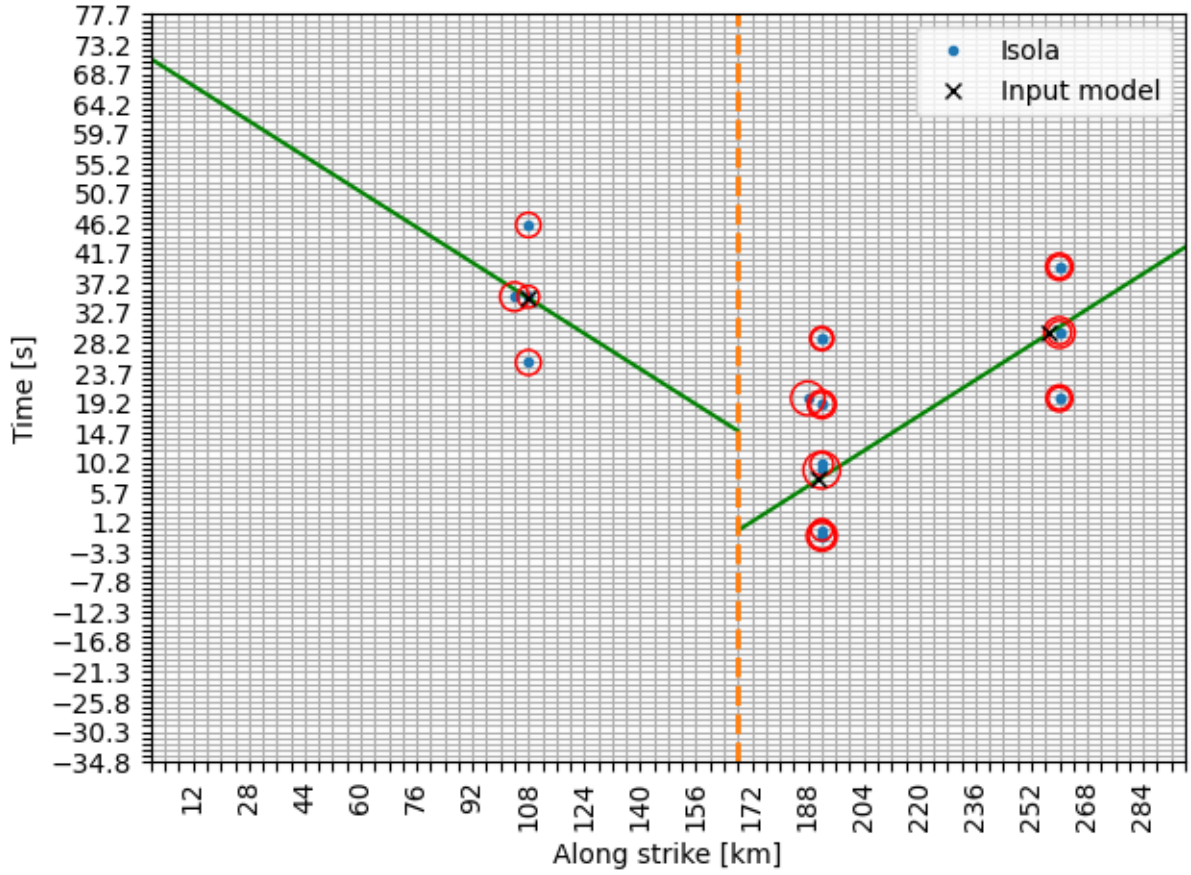

Fig. 10: **Test 6 (Point-like model. Inversion with Isola "slow", free full MT mechanisms, triangle 20-s function).**

Continuous slip models

TEST 7: SLOW Isola model, FIXED mechanisms (two), DELTA function

Type of inversion: Fixed mechanism (s/d/r = 30/90/0, and 60/90/0 on the SW and NE segment, respectively); the transition between the segments is at trial position No. 38

Subevent time function: Delta function

Isola type: Slow

Number of searched subevents: 90

Number of trial source positions: 75

Temporal grid search: (-5.1, 80.1) s with step of 0.9 s

Frequency range: (0.01, 0.05) Hz

Details in supplement: Tab. S7, Fig. S19 - S20

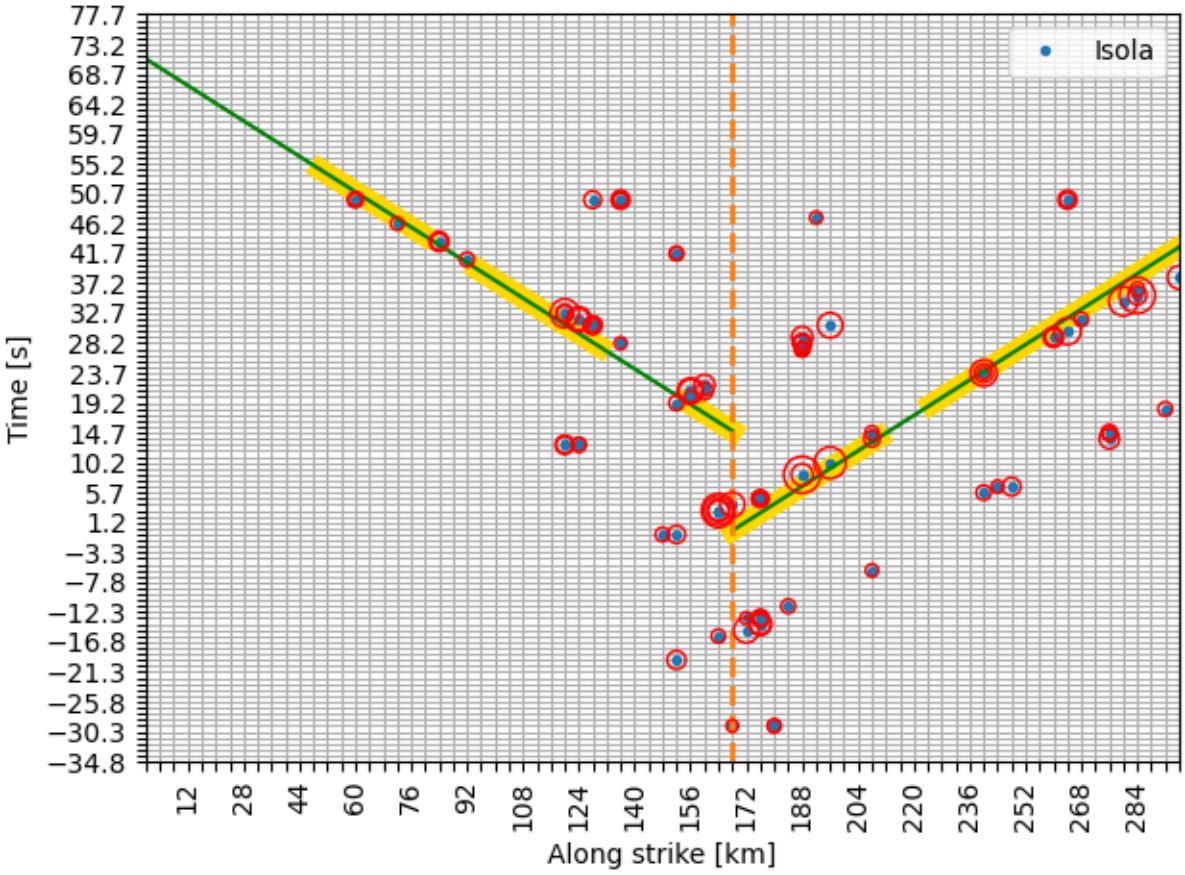

Fig. 11: **Test 7 (Continuous model. Inversion with Isola "slow", prescribed focal mechanisms, delta function).** Yellow stripes denote the approximate extent of the major slip asperities A-F of the input model of Fig. 4. The remaining symbols are the same as in Fig. 5.

TEST 8: SLOW Isola model, DC constrained, DELTA function

Type of inversion: DC constrained; the transition between the segments is at trial position No. 38

Subevent time function: Delta function

Isola type: Slow

Number of subevents: 90

Number of trial source positions: 75

Temporal grid search: (-5.1, 80.1)s with step of 0.9s

Frequency range: (0.01, 0.05)Hz

Details in supplement: Tab. S8, Fig. S21 - S22

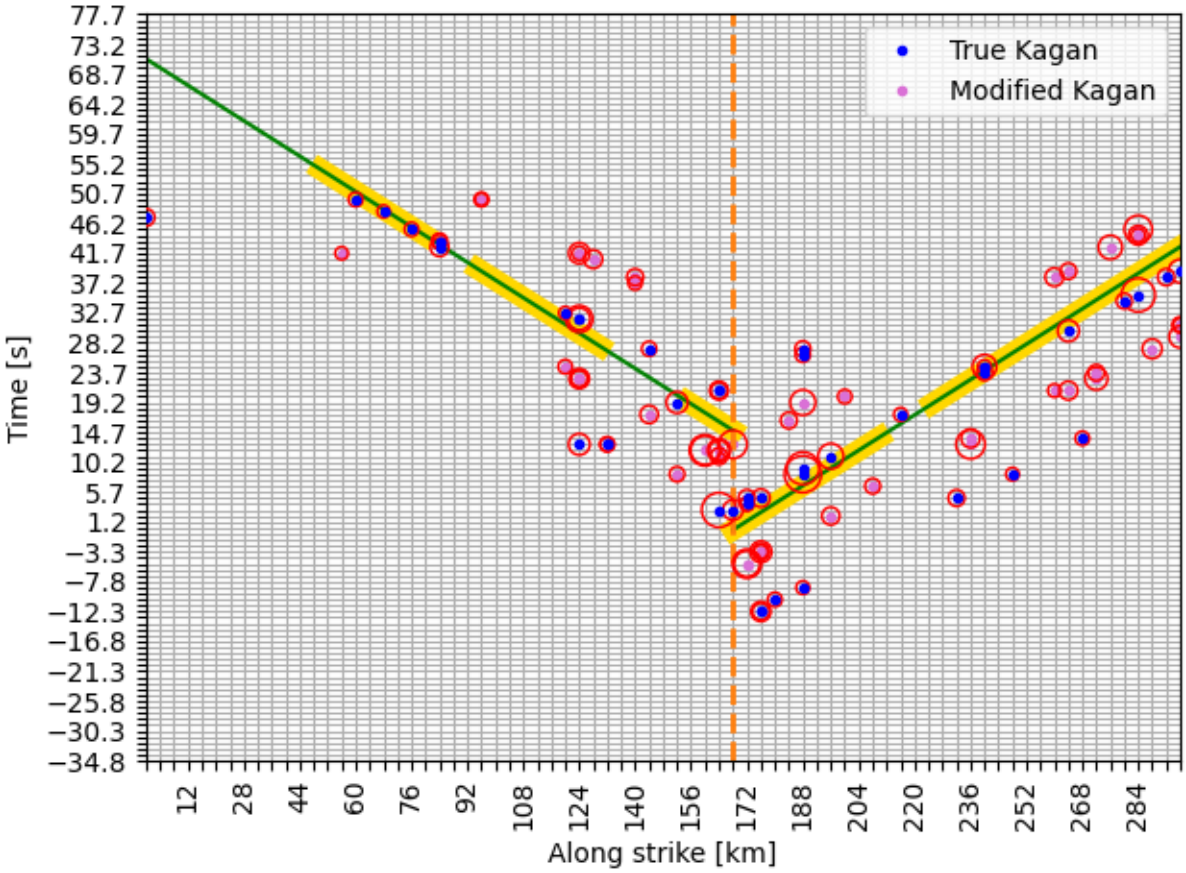

Fig. 13a: **Test 8 (Continuous model. Inversion with Isola "slow", free DC-constrained mechanisms, delta function).** The Kagan angle is shown according to the legend. The remaining symbols are the same as in Fig. 11.

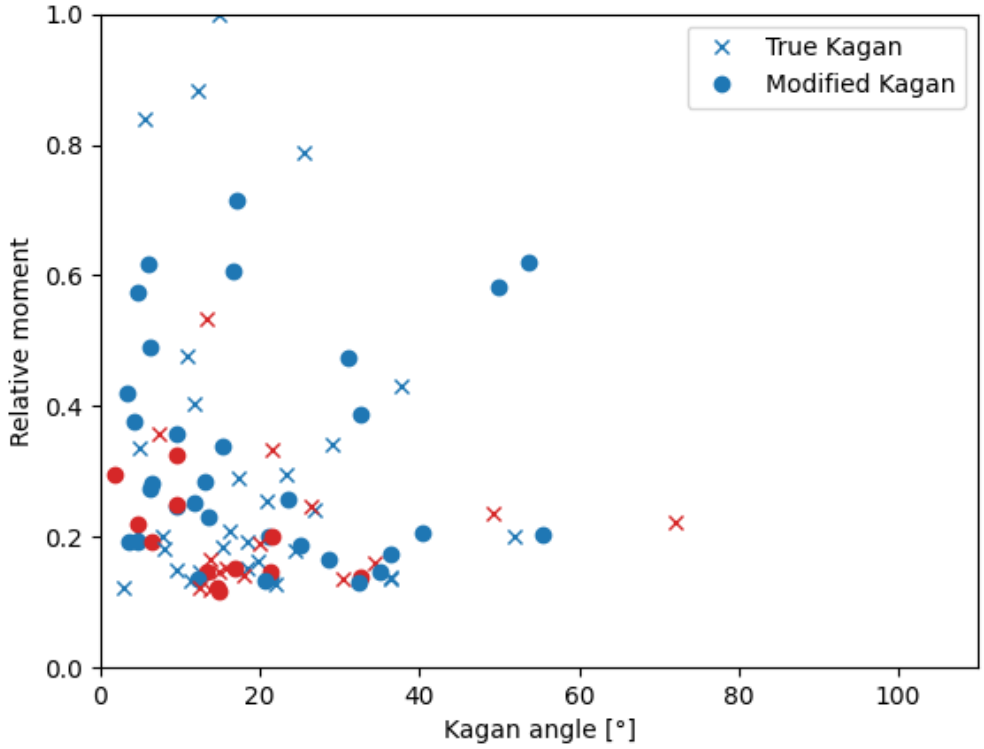

Fig. 13b: **Test 8 (Continuous model. Inversion with Isola "slow", free DC-constrained mechanisms, delta function).** Relative moment of subevents versus their Kagan angle deviation from the input model. The blue and red symbols refer to the NE and SW segments, respectively. For an explanation of the modified Kagan angle, see Introduction.

TEST 9: SLOW Isola model, FULL MT, DELTA function

Type of inversion: Full MT; the transition between the segments is at trial position No. 38

Subevent time function: Delta function

Isola type: Slow

Number of subevents: 90

Number of trial source positions: 75

Temporal grid search:: (-5.1, 80.1)s with step of 0.9s

Frequency range: (0.01, 0.05) Hz

Details in supplement: Tab. S9, Fig. S23 - S24

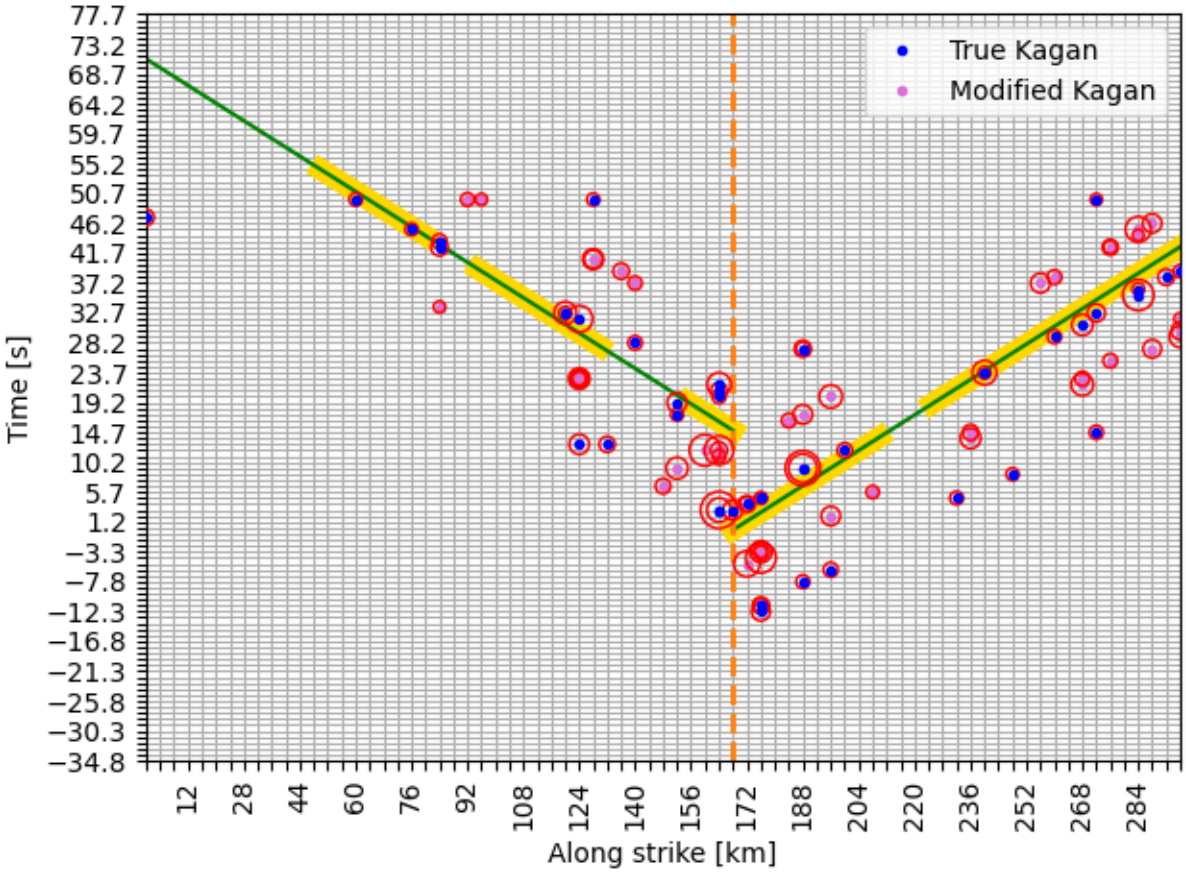

Fig. 14a: **Test 9 (Continuous model. Inversion with Isola "slow", free full MT mechanisms, delta function).** The Kagan angle is shown according to the legend. The other symbols are the same as in Fig. 11.

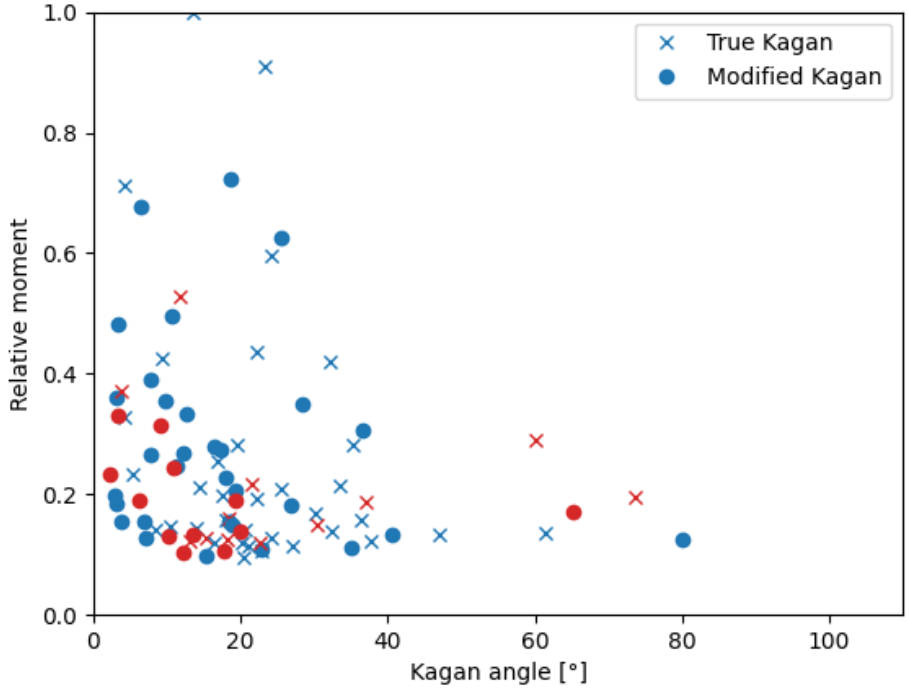

Fig. 14b: **Test 9 (Continuous model. Inversion with Isola "slow", free full MT mechanisms, delta function).** Symbols as in Fig. 13b.

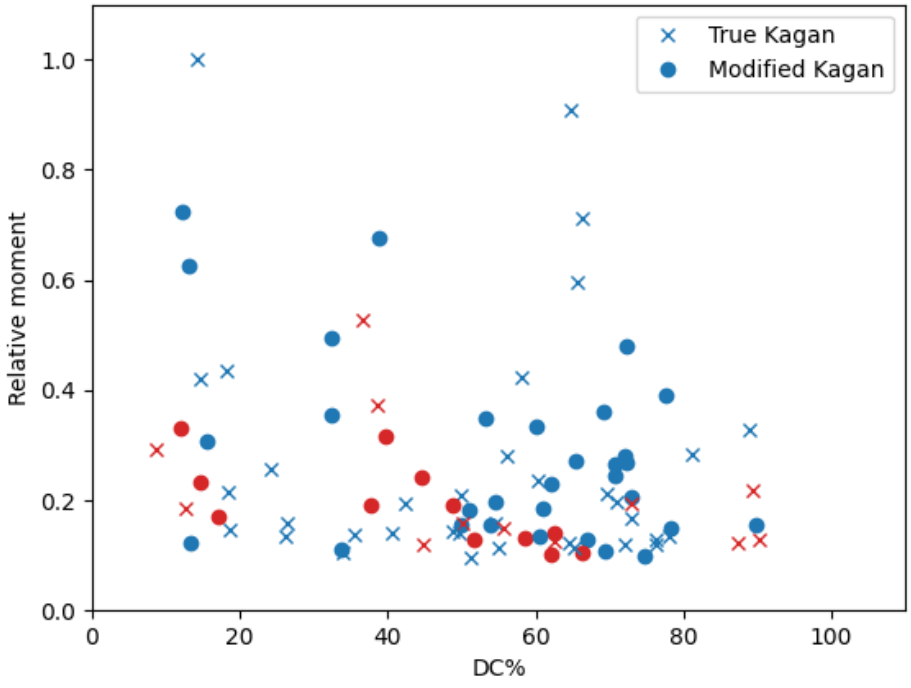

Fig. 14c: **Test 9 (Continuous model. Inversion with Isola "slow", free full MT mechanisms, delta function).** Relative moment of subevents versus their DC percentage (the input model had DC=100%). The blue and red symbols refer to the NE and SW segments, respectively. For an explanation of the modified Kagan angle, see Introduction.

TEST 10: FAST Isola model, FIXED mechanisms (two), DELTA function

Type of inversion: Fixed mechanism (s/d/r = 30/90/0, and 60/90/0 on the southern and northern segment, respectively); the transition between the segments is at trial position No. 38

Subevent time function: Delta function

Isola type: Slow

Number of subevents: 90

Number of trial source positions: 75

Temporal grid search: (-5.1, 80.1)s with step of 0.9s

Frequency range: (0.01, 0.05) Hz

Details in supplement: Tab. S10, Fig. S25 - S26

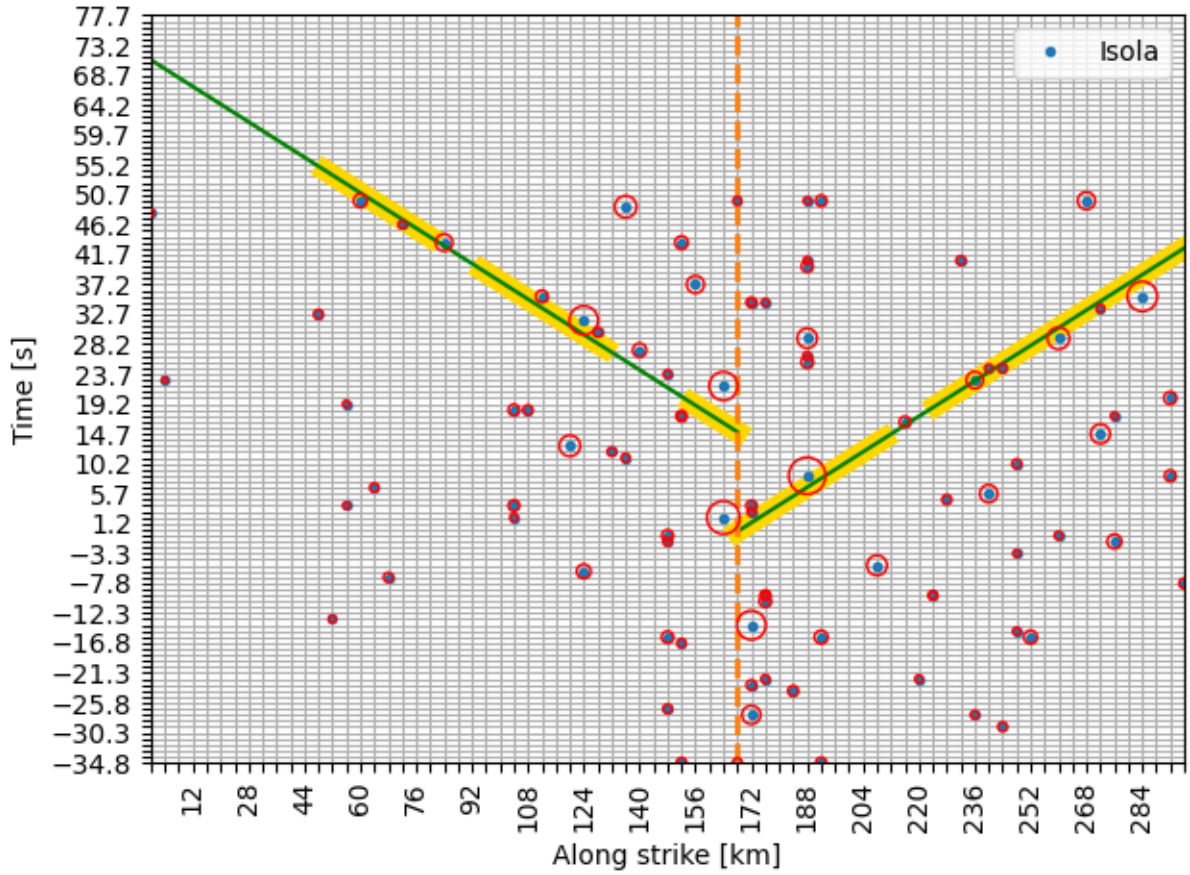

Fig. 15: **Test 10 (Continuous model. Inversion with Isola "fast", prescribed focal mechanisms, delta function).** The symbols are the same as in Fig. 11.

Conclusions

1. In this study, we have investigated two main slip models: point-like and continuous. Results for the continuous slip models are more important for real-data interpretations, so we focus on them.
2. Besides subevents following the input model (the red circles near the green lines, i.e. the subevents indicating correct rupture speed), we find many temporal artifacts (the circles below and above the green lines).
3. Most temporal artifacts, but not all, have small relative moments (< 0.4).
4. If all small subevents are ignored, because they can be potential artifacts, we obtain very few subevents on the SW segment, where input slip was low (asperity F). This is a serious limitation for assessing rupture history on the SW segment.
5. The slip asperities A-D are well represented in the inversion as subevents with the largest relative moments; the asperity F is less well resolved.
6. Subevents with free DC constrained mechanism, or full MT, produce false mechanisms, quantified with Kagan angle [that differs from 0] and DC percentage [that differs from 100%]. Even subevents of the largest relative moment (= 1) have a non-zero Kagan angle, e.g. K=20°. Many subevents, even those with relatively high relative moment (> 0.6), fail to correctly resolve the 180° ambiguity of the rake angle, so their Kagan angle had to be modified. Even after Kagan angle modifications, a few subevents still have K > 60°. Subevents of smaller relative moments are numerous, their modified Kagan angle is mostly < 30- 40°, which is still a good agreement with the input model.
7. Even the largest subevents have a very large deviation of DC from 100% if the mechanism is not fixed or DC-constrained. Large non-DC artifacts are observed not only for subevents that require Kagan angle modification. The SW and NE segments do not differ regarding the occurrence of large Kagan angles and low DC%.

The overall summary is that the inversion artifacts are numerous. They include false non-DC components [very serious], false focal mechanisms [not as severe if the possible 180° rake ambiguity is considered], and false subevent times. In the test cases with continuous slip models, the inversion is most difficult for the SW segment, mainly on asperity F. It remains to be clarified whether the false times of the subevents correlate with the false focal mechanisms (whose Kagan angle had to be modified). Subevents of false times represent the main limitation of the rupture-speed assessment. The problem is not in the absence of subevents of nearly exact times (those on the green lines) but in the existence of additional (false) subevents with incorrect times. In the NE segment, all subevents (correct and false together) form a wide “stripe”, parallel to the green line. Being parallel to the green line, the stripe indicates the correct rupture speed, but the speed value cannot be retrieved by a simple least-squares straight-line approximation. On the SW segment and near the corner between the SW and NE segments, the inversion is the most obscured.

Acknowledgment: The location of the strong motion stations was taken from the Disaster and Emergency Management Authority of Türkiye (AFAD – TK), https://tdvms.afad.gov.tr. The author thanks the Department of Geophysics of the Faculty of Mathematics and Physics, Charles University, for financial support. The work was performed under the guidance of Jiri Zahradnik.

Appendix A: Supplementary material

Supplementary material to this article can be found online at https://doi.org/10.6084/m9.figshare.27225258.v1.

References

Acarel, D., Cambaz, M. D., Turhan, F., Mutlu, A. K. & Polat, R. (2019). Seismotectonics of Malatya fault, Eastern Turkey. *Open Geosci.* 11, 1098–1111.

Coutant, O. (1989). Program of numerical simulation AXITRA, Research Reports LGIT. University of Joseph Fourie, Grenoble, France.

Čejka, F., Zahradník, J., Turhan, F., Sokos, E., Gallovič, F. (2023). Long-period directivity pulses of strong ground motion during the 2023 Mw7.8 Kahramanmaraş earthquake. *Commun. Earth Environ.* 4, 413, https://doi.org/10.1038/s43247-023-01076-x.

Gallovič, F., Brokešová, J. (2007). Hybrid k-squared source model for strong ground motion simulations: introduction. *Phys. Earth Planet. Inter.* 160, 34‑50.

Kagan, Y. Y. (1991). 3-D rotation of double-couple earthquake sources. *Geophysical Journal International*, *106*(3), 709–716. https://doi.org/10.1111/j.1365-246X.1991.tb06343.x

Zahradník, J., and F. Gallovič (2010). Toward understanding slip inversion uncertainty and artifacts, *J. Geophys. Res.*, 115, B09310, doi:10.1029/2010JB007414.

Zahradník, J., and E. Sokos (2018). ISOLA code for multiple-point source modeling –review. In: "*Moment Tensor Solutions - A Useful Tool for Seismotectonics" (S. D'Amico, Ed.), Springer*. Available at https://geo.mff.cuni.cz/~jz/

Zahradník, J., F. Turhan, E. Sokos, and F. Gallovič (2023). Asperity-like (segmented) structure of the 6 February 2023 Turkish earthquakes. *EarthArXiv*, https://doi.org/10.31223/X5T666.